



HAL
open science

Core-derived historical records of suspended sediment origin in a mesoscale mountainous catchment: the Bléone River French Alps

O. Navratil, O. Evrard, Michel Esteves, Sophie Ayrault, Irene Lefevre, Cédric Legout, Jean-Louis Reyss, Nicolas Gratiot, Julien Nemery, Nicolle Mathys, et al.

► To cite this version:

O. Navratil, O. Evrard, Michel Esteves, Sophie Ayrault, Irene Lefevre, et al.. Core-derived historical records of suspended sediment origin in a mesoscale mountainous catchment: the Bléone River French Alps. *Journal of Soils and Sediments*, 2012, 12 (9), pp.1463-1478. 10.1007/s11368-012-0565-2 . halshs-01222790

HAL Id: halshs-01222790

<https://shs.hal.science/halshs-01222790>

Submitted on 26 May 2020

HAL is a multi-disciplinary open access archive for the deposit and dissemination of scientific research documents, whether they are published or not. The documents may come from teaching and research institutions in France or abroad, or from public or private research centers.

L'archive ouverte pluridisciplinaire **HAL**, est destinée au dépôt et à la diffusion de documents scientifiques de niveau recherche, publiés ou non, émanant des établissements d'enseignement et de recherche français ou étrangers, des laboratoires publics ou privés.

1 SEDIMENTS, SEC 3 • HILLSLOPE AND RIVER BASIN SEDIMENT DYNAMICS •
2 RESEARCH ARTICLE

3

4 **Core-derived historical records of suspended sediment origin in a mesoscale**
5 **mountainous catchment: the Bléone River, French Alps**

6

7 **Oldrich Navratil • Olivier Evrard • Michel Esteves • Sophie Ayrault • Irène Lefèvre •**
8 **Cédric Legout • Jean-Louis Reyss • Nicolas Gratiot • Julien Nemery • Nicole Mathys •**
9 **Alain Poirel • Philippe Bonté**

10

11 O. Navratil (✉) • M. Esteves • C. Legout • N. Gratiot • J. Nemery

12 LTHE - IRD/Université Grenoble 1/G-INP/CNRS, BP 53, 38041 Grenoble Cedex 9, France

13 e-mail: navratiloldrich@gmail.com

14

15 O. Navratil • N. Mathys

16 Irstea, UR ETGR, Erosion torrentielle neige et avalanches, 38402 St-Martin-d'Hères, France

17 e-mail: navratiloldrich@gmail.com

18

19 O. Evrard (✉) • S. Ayrault • I. Lefèvre • J.-L. Reyss • P. Bonté

20 Laboratoire des Sciences du Climat et de l'Environnement (LSCE/IPSL) – Unité Mixte de

21 Recherche 8212 (CEA, CNRS, UVSQ), 91198 Gif-sur-Yvette Cedex, France

22 e-mail: olivier.evrard@lsce.ipsl.fr

23

24 A. Poirel

25 EDF-DTG, Electricité de France, Grenoble Cedex 9, France

26

27 (✉) **Corresponding authors:**

28 Oldrich Navratil

29 e-mail: navratiloldrich@gmail.com

30 and

31 Olivier Evrard

32 e-mail: olivier.evrard@lsce.ipsl.fr

33

34

35 **Abstract**

36 **Purpose:** Quantifying suspended sediment fluxes and dynamics across mountains and
37 identifying the origin of sediment in severely eroded areas are of primary importance for an
38 equilibrate management of water resources. This contribution aims at generalising previous
39 results of suspended sediment fingerprinting obtained during the 2007-2009 period in a
40 mesoscale Alpine catchment, the Bléone River (905 km²) and to possibly check their validity
41 throughout the second half of the 20th century.

42 **Materials and methods:** Sediment fingerprinting based on elemental geochemistry and
43 radionuclide measurements was conducted on a sediment core collected in an alluvial
44 floodplain at the basin outlet. This technique was combined with long hydro-sedimentary
45 time-series to reconstruct the origin of suspended sediment that deposited at this location
46 throughout the last 50 years.

47 **Results and discussion:** Hydro-sedimentary interpretation of sedimentation based on
48 historical hydrological databases corroborates core dating obtained with ¹³⁷Cs and ²¹⁰Pb_{xs}
49 activity measurements. Black marls and (marly) limestones provided the bulk of sediment
50 throughout the sequence (40% and 22%, respectively), while they only occupies 10% of the
51 total catchment area. However, we also showed the occurrence of major floods carrying large
52 quantities of sediment originating from Quaternary deposits and conglomerates (25% and
53 16%, respectively). The variability of sediment sources throughout the sequence may reflects
54 the spatial variability of rainfall within the catchment, depending on air mass origin.
55 However, the relatively homogeneous sediment composition throughout the sequence
56 confirms that core-derived information is representative of large-scale flood events.

57 **Conclusions:** In conclusion, these results are consistent with the ones obtained in previous
58 studies. They also outline the need to take account of the entire grain size range of fine
59 sediment to provide an overall picture of sediment sources and transfers within highly erosive
60 catchments. This study finally emphasize the relevance of using archive data to validate
61 sediment fingerprinting generally conducted during short monitoring programs across larger
62 time period and large widespread floods.

63

64 **Keywords** Braided river • Erosion • Geochemistry • Radionuclide • Sediment core •
65 Sediment fingerprinting

66

67

68 **1 Introduction**

69 In mountainous regions, hillslope erosion and mass movements supply large quantities of
70 fine-grained sediment ($< 63 \mu\text{m}$) to rivers where they generally cause numerous
71 environmental and economical problems, such as reservoir siltation and operational problems
72 for hydroelectric power plants (e.g., Valero-Garcés et al. 1999). An excess of sediment supply
73 can also lead to an increase in water turbidity, eutrophication and degradation of riverine
74 habitats in lowland areas (e.g. Owens et al. 2005). Furthermore, although suspended sediment
75 conveys the biogenic elements required by all the living organisms, the finest fraction (< 63
76 μm) is also one of the main vectors of contaminant transfer (e.g., PCBs, heavy metals) within
77 catchments (Owens and Walling 2003; Collins et al. 2005).

78 The Rhône River that flows across Switzerland and France has become the main sediment
79 supplier to the Mediterranean Sea since damming of the Nile River (Sempéré et al. 2000).
80 Downstream reaches of this river are confronted with particularly severe contamination and
81 siltation problems (Antonelli et al. 2008; Sicre et al. 2008). Previous studies hypothesised that
82 a significant part of sediment probably originated from the badland areas constituted of black
83 marls and located in the Durance River catchment (e.g. Pont et al. 2002; Di Giovanni et al.
84 2002). During the 3-year STREAMS (Sediment TRansport and Erosion Across MountainS)
85 research project funded by the French Research Agency, a large hydro-sedimentary database
86 was compiled in the Bléone River catchment (905 km²) which is one of the main contributor
87 of sediment to the Durance River (Mano et al. 2009). The catchment is equipped with 7
88 hydrometric stations at intermediary scales (i.e., 10–1000 km²). Each station is characterised
89 with high frequency acquisition of discharge and turbidity, and suspended sediment sampling
90 during floods. This network provided a useful complement to the existing installations of the
91 Draix Observatory that have been used since 1985 to investigate sediment dynamics in small
92 ($< 1 \text{ km}^2$) severely eroded headwater catchments (Mathys et al. 2003). Sediment
93 fingerprinting studies were conducted in this catchment to better understand the dynamics and
94 to define the origin of the suspended sediment in the catchment. Evrard et al. (2011) and
95 Navratil et al. (2012) outlined the very large spatial and temporal variability of sediment
96 sources and exports during this study period. The preliminary results showed that 80% of
97 suspended sediment was produced by floods generated by widespread low-intensity rainfall
98 across the catchment. Such result corroborates the conclusions of Duvert et al. (2010, 2011).
99 Furthermore, the analyses of several 1-2 yrs return period floods and one major flood (10 yrs-
100 return period flood) that occurred in a subcatchment confirmed the important contribution of
101 black marls (up to 70%) to sediment transported in rivers, although this substrate only
102 occupies ca. 10% of the total catchment surface. Sediment exports generated by local

103 convective storms varied significantly at both intra- and inter-flood scales, because of spatial
104 heterogeneity of rainfall. However, black marls/marly limestones contribution remained
105 systematically high. In contrast, widespread flood events that generate the bulk of annual
106 sediment supply at the outlet were characterised by a more stable lithologic composition and
107 by a larger contribution of limestones/marls, Quaternary deposits and conglomerates (Navratil
108 et al. 2012).

109 In order to validate those findings over a longer time period and to enlarge the scope of
110 our fingerprinting study to a larger set of weather and flood conditions, we investigated the
111 evolution of suspended sediment origin and dynamics over a 50-year period from the severely
112 eroded Bléone river catchment (905 km²). To this end, we collected a sediment core in the
113 alluvial floodplain at the Bléone catchment outlet. Long-term meteorological and
114 hydrological datasets were used to interpret the structure of this core and to associate the
115 sediment deposits with different hydrological periods. Radionuclide and elemental
116 geochemistry properties were then measured on the core sediment samples. A mixing model
117 was finally used to trace the origin of suspended sediment transported during a selection of
118 past large floods.

119

120

121 **2 Study area**

122 The Bléone catchment (905 km²; lat.: 44°05'34''N, long.: 06°13'53''E), with altitude
123 ranging between 405 and 2961 m A.S.L. (Above Sea Level), is a mountainous Alpine
124 catchment located in the Durance River district, in southeastern France (Fig. 1). The
125 catchment is characterised by a dendritic drainage network dominated by the Bléone River
126 and several tributaries, among which the Bès River (233 km²-subcatchment) is the most
127 important. Forest is by far the main land use in the catchment (44% of the total catchment
128 surface; Table 1). The lithology mainly consists of marls, molasses and limestones, with large
129 areas of exposed Cretaceous and Jurassic black marls, as well as Lias marly limestones (Fig.
130 2). Geological information was derived from a digitised 1:50,000 spatially-distributed
131 geological map of the catchment provided by the French Geological Survey (BRGM). Eroded
132 surfaces (covering 11% of the total Bléone catchment area, see Fig. 2) were delineated in a
133 GIS using aerial photographs taken during flight campaigns conducted in 2004 by the French
134 National Geographic Institute (IGN). Eroded surfaces cover a mean surface of 0.45 km²
135 (between 811 m² and 1.85 km²) and were classified into three groups: debris slope areas (22%
136 of the eroded areas), sheet and rill erosion areas (48%), and gully erosion areas (30%). Areas

137 covered by black marls are strongly affected by erosion and are characterized by a badland
138 morphology (Mathys et al. 2005).

139 The climate is transitional and undergoes mountainous and Mediterranean influences. Mean
140 annual temperature ranges between 12–13°C at 400 m A.S.L., with high temperature
141 variations between summer and winter (about 18°C). Mean annual rainfall in the catchment
142 varies between 600–1200 mm at 400 m A.S.L. According to local archives (*Archives*
143 *Départementales des Alpes de Haute Provence*), the largest historical flood at the basin outlet
144 is reported to have occurred in July 1854, with a peak discharge estimated at $\sim 1,100 \text{ m}^3 \text{ s}^{-1}$
145 (Sogreah, 2005). Over the past decades, the maximum specific peak discharges were
146 significantly higher in the Bès River subcatchment (165 km²) than in other similar catchments
147 of the Southern French Alps (Fig. 3c): $3.6 \text{ m}^3 \text{ s}^{-1} \text{ km}^{-2}$ for the Bès River, against less than 1.4
148 $\text{m}^3 \text{ s}^{-1} \text{ km}^{-2}$ in other catchments. This subcatchment has therefore a very specific behaviour.
149 Furthermore, floods that occurred in this area from 1960 to 2009 were characterised by a
150 strong seasonality. Most of the floods occurred in autumn (see Fig. 3a). South or South-
151 Western atmospheric fluxes originating from the Mediterranean Sea and characterised by
152 humid and warm air flows provide the bulk of annual rainfall in this region. They triggered
153 most of the largest floods observed since 1960 (see Fig. 3b). The presence of a widespread
154 depression centered on France is also associated with heavy rainfall in the entire country and
155 generates large and widespread floods at the basin scale. In contrast, Western weaker
156 depressions coming from the Atlantic Ocean generally dry up over the first French mountain
157 ranges (i.e., Massif Central and Pyrénées), so that they only provide low-intensity rainfall
158 when they reach the Southern Alps. Northern and North-Western fluxes occur when the
159 Azores High is located at high latitudes; midlatitude cyclones can then arrive from the
160 Northern Alps and produce the bulk of the snow cover. Eastern fluxes are associated with a
161 high pressure cell standing over central Europe. Contact between this cold and dry air mass
162 with the Mediterranean air mass can trigger particularly heavy storms over the Southern Alps
163 in spring and summer. Finally, when high pressure cells dominate in the region, local
164 convective storms can also occur due to local air mass instability (Gottardi 2009). These
165 storms mostly occur between June and September. They are associated with heavy downpours
166 that may trigger flash floods and debris flows that are otherwise restricted to small headwater
167 streams.

168

169

170 **3 MaterialS and methodS**

171 **3.1 Coring site**

172 A 3-meter long sediment core (5-cm diameter) was collected on 26 November, 2009 with
173 a Cobra corer in the Bléone River floodplain, upstream of the Malijai dam close to the outlet
174 (see Fig. 1b; 905 km²). Coring was conducted in collaboration with the *Laboratoire de*
175 *Géophysique Interne et Tectonophysique* (LGIT) and the *Laboratoire des Sciences de*
176 *l'Environnement* (LSE). The sampling site was selected on a vegetated bar composed of very
177 fine sediment, adjacent to the river channel, and located about 1 meter above the mean
178 floodplain level. During floods, water level and flow velocity are controlled so as to ensure
179 good operating conditions for the dam. In the recent period, we observed that the floodplain
180 was systematically submerged during the largest floods. There was no evidence of bank
181 erosion in the vicinity of the coring site. We therefore hypothesize that this site located within
182 the dam reservoir has underwent a slow sedimentation since the dam building.
183 Malijai dam was built by the French national electricity producer (EDF) in 1962. During base
184 flow periods, the dam is closed to divert part of the clear water into a canal. To limit supply of
185 sediment and associated substances to the downstream Berre lagoon (Accornero et al. 2008),
186 French authorities fixed a maximal suspended sediment concentration that can be delivered to
187 the canal, which leads to extra management costs for the company exploiting the power
188 plants. Consequently, during floods, the dam is opened manually in order to divert water and
189 sediment into the main channel. Sediment siltation mainly occurs during large floods (>1-2
190 yrs return period) in the reservoir area where we sampled the sediment core. From 1962
191 onwards, the dam has accumulated sediment, whereas resuspension of fine sediment and
192 bedload only occurred in the middle part of the active river channel (see Fig. 1b).

193

194 **3.2 Stratigraphic structure of the sediment core**

195 In this study, we used X-ray measurements and visual observations to outline the
196 stratigraphic structure of the core, i.e. the succession of flood deposits since the Malijai dam
197 construction (1962).

198 The core was X-rayed at the *Eaux Claires* Hospital of Grenoble, with the aim to associate
199 specific densities with grey level intensities (de Montety et al. 2003). Longitudinal image
200 resolution was 2 mm; mean and standard deviation of grey level intensities were then
201 measured in each section (i.e. horizon) within a 2 by 2 cm window centered on the core axis.
202 Grey shades are considered to reflect the density of sediment as the grey-scale intensity of an
203 X-ray image is proportional to beam attenuation of the incident X-ray (Lofi and Weber 1999).

204 The grey intensity variations in that core would therefore undoubtedly reflect the succession
205 of flood deposits (i.e., varves).

206 Then, the sediment core was cut into two longitudinal parts, photographed, and subsampled
207 based on two strategies: (1) sections were made following the stratigraphic structures of
208 varves detected by X-ray analysis and visual observation, on the first half of the core; (2) 2-
209 cm wide sections were cut on the second half of the core. Sediment samples were ground to a
210 fine powder and dried at 105°C for 2 hours.

211 Then, we measured the grain-size of a selection of core samples to analyse the inter- and
212 intra- varve variations of grain-size fraction. Subsamples were analysed with a Malvern®
213 particle laser sizer after 7-min of stirring and sonication. Grain size distributions and statistics
214 were computed with Gradistat software (Blott and Pie 2001).

215

216 **3.3 Origin of fine sediment**

217 ***3.3.1 Soil and core sediment sampling***

218 Representative soil samples were collected in the Bléone basin to characterize
219 potential source materials (see Evrard et al. 2011 for details). They were taken mostly on
220 colluvial toeslopes adjacent to the drainage network to be representative of material eroded
221 from adjacent hillslopes. Soil samples were dried at 105°C and disaggregated prior to
222 analysis. As the core sediment samples have a finer grain size than the soil samples (i.e.,
223 potential sediment sources), we sieved this source material to <63 µm before conducting
224 radionuclide and geochemical analyses (Navratil et al. 2012).

225 We used the 2-cm core section samples (n = 92 for the core dating and n = 34 for the sediment
226 fingerprinting) to cover the entire sequence of sediment deposit. The sediment samples were
227 dried at 40°C, disaggregated and sieved to 63µm.

228

229 ***3.3.2 Measurement of radionuclide and elemental geochemistry***

230 In total, we measured gamma-emitting radionuclide activity in 92 core samples and
231 the 150 source samples. Sediment was placed in a counting box when there was sufficient
232 material (≥10 g). Radionuclide activities (²⁴¹Am, ¹³⁷Cs, ⁴⁰K, ²¹⁰Pb, ²²⁶Ra, ²²⁸Ra, ²³⁴Th, ²²⁸Th)
233 were determined by gamma-spectrometry using the very low-background coaxial N- and P-
234 types GeHP detectors (Canberra / Ortec / EurisyS) available at the *Laboratoire des Sciences*
235 *du Climat et de l'Environnement* (Gif-sur-Yvette, France). Efficiencies and background levels
236 of the detectors were periodically controlled with internal and IAEA (International Atomic
237 Energy Agency) soil and sediment standards (Evrard et al. 2010; Evrard et al. in press). When

238 there was < 10 g sediment available, filters were placed in tubes and counting was conducted
239 at the *Laboratoire Souterrain de Modane* (LSM; CNRS-CEA) under the French Alps, using a
240 very low background, high-efficiency well-type Ge detector (Reyss et al. 1995).

241 For the measurement of elemental geochemistry, dried subsamples (c. 80 mg) of selected 2-
242 cm core sections (n = 34) were analysed by inductively coupled plasma – mass spectrometry
243 (ICP-MS; XII CCT Series, Thermo Electron), in solutions containing 0.2 g of solid L⁻¹. The
244 sediment total digestion procedure is described by Le Cloarec et al. (2011). Concentrations
245 were determined for five major (Al, K, Fe, Mg, Ti) and thirteen trace (Ag, Ba, Cd, Co, Cr, Cu,
246 Mn, Ni, Pb, Sb, Tl, V, Zn) elements. The accuracy of the elemental concentration
247 determination was evaluated through the repetitive analysis of the certified reference material
248 SL-1 (lake sediment, AIEA, Vienna, Austria). The obtained values (n=4), agreed with the
249 certified concentrations, when available. Certified values are not available for Ag, Al, Ca, Mg
250 and Tl. The accuracy of the determination of these four elements in SL-1 was cross-checked
251 with values determined by neutron activation analysis (Ayrault et al. 2010; Evrard et al.
252 2011). Analytical uncertainties associated with this method did not exceed 20 and 10% for
253 major and trace element determination, respectively. Analysis of source material is described
254 in detail in Navratil et al. (2012).

255

256 ***3.3.3 Selection of fingerprints and design of a mixing model***

257 Based on the French Geological Survey (BRGM) map of the catchment (see Fig. 2),
258 we grouped the geological classes represented on the map and corresponding to our sediment
259 source samples types into 5 classes: (1) marly limestones; (2) limy marls; (3) conglomerates;
260 (4) Quaternary deposits; (5) black marls (see Evrard et al. 2011). As described by Navratil et
261 al. (2012), we selected 10 fingerprinting properties that can discriminate between these five
262 different sediment sources. Among them, 6 properties were sufficient to design the optimum
263 composite fingerprint. Only one geogenic radionuclide was pointed out (²²⁶Ra). The other
264 selected fingerprints were V, Ni, Mn, Sb and Cu. Then, we constructed a Monte Carlo mixing
265 model as detailed by Navratil et al. (2012) in order to quantify the contribution of each
266 sediment source to the core sediment samples.

267

268 **3.4 Core dating**

269 Dating of the sediment cores relied on the measurement of two radionuclides (i.e.,
270 ¹³⁷Cs and ²¹⁰Pb_{xs}) that strongly sorb onto fine sediment (Owens et al. 1999). ¹³⁷Cs was used as
271 an event-tracer, whereas ²¹⁰Pb_{xs} provided the sediment age (Appleby 2000). Both

272 radionuclides are gamma emitters and they can be detected without any previous chemical
273 treatment of sediment.

274 ^{137}Cs is an artificial radionuclide ($t_{1/2} = 30$ years) produced by the thermonuclear bomb testing
275 conducted between the 1950s and the 1980s (with a maximum input in 1963) and, depending
276 on local weather conditions, after the Chernobyl accident in 1986. ^{137}Cs is now stored in soils,
277 and this ^{137}Cs stock decreases by radioactive decay and by fine sediment transfer to the rivers.
278 Uncertainty on measurements was ca. 0.5%, and the detection limits reached 0.3 Bq kg^{-1} .

279 ^{210}Pb is a natural radionuclide ($t_{1/2} = 22.3$ years) which is a decay product of ^{238}U ($t_{1/2} = 4.5 \times$
280 10^9 years). ^{238}U decays through a series of short-lived nuclides (e.g., ^{226}Ra and ^{222}Rn). ^{222}Rn is
281 a gas that partly remains *in situ*, forming “supported” ^{210}Pb , and that partly escapes to the
282 atmosphere, forming “excess” ^{210}Pb , which reaches the soil surface by wet and dry fallout. It
283 then strongly sorbs to soil particles. The activity in “excess” ^{210}Pb was calculated by
284 subtracting the supported activity (determined using a ^{238}U daughter, i.e. ^{214}Bi) from the total
285 activity of ^{210}Pb . Uncertainty on measurements was thus higher than for ^{137}Cs (ca. 10%).

286 Sedimentation rates were then calculated based on the Constant Rate Supply (CRS) model
287 (Appleby and Oldfield 1983).

288

289 **3.5 Climatological and hydro-sedimentary databases**

290 Classically, core interpretation involves a count-from-the-top correlation of the
291 individual flood deposits with flood events that resulted in overbank deposition (e.g. Hobo et
292 al. 2010). However, evident difficulties prevented to associate each individual varve with
293 individual flood events: (1) the context of this study (mountainous river with flash floods,
294 complex sedimentation due to dam functioning) and (2) the lack of long-term water-
295 level/discharge time-series available at the coring location. We therefore analysed the
296 correlation between the stratigraphic structure of the core (succession of varve thickness) and
297 the inter-annual hydro-meteorological variations. Given the lack of discharge data available at
298 the Bléone River outlet, we compiled data from various sources available at different spatial
299 scales and temporal resolutions to interpret the flood deposits at the Bléone River outlet:
300 databases of rainfall time-series, discharge and suspended sediment concentration time-series
301 and historical floods and mass movements.

302 Ten rain-gauges managed by the *Laboratoire d'étude des Transferts en Hydrologie et*
303 *Environnement* (R1–R5) and the French *Cemagref* research agency (R6–R10) provided
304 continuous precipitation records (see Fig. 1; Table 1). Five meteorological stations managed
305 by the French meteorological office (i.e., *Météo France*) provided rainfall depths and

306 durations, snow depth, temperature as well as information on the occurrence of storm or hail
307 events (R11–R15). Four of them provided daily rainfall for the 1960-2009 period (R11, R12,
308 R14, R15; Table 1). These last stations only provided daily records (with the exception of one
309 station, i.e., R12, providing hourly records). Altogether, these data provided good information
310 about spatial and temporal variability of rainfall at the Bléone River basin scale.

311 Discharge, suspended sediment concentration (SSC) and yields (SSY) were measured at 1-h
312 time steps by *EDF* at the Malijai station during the 2001-2003 and 2007–2009 periods (Table
313 1). Discharges were measured on the Bès River at Pérouré station (165 km²; see Fig. 1) during
314 the 1963–2009 period. SSC have been measured with turbidimeters since October 2007 – see
315 Navratil et al. (2010) and Navratil et al. (2011) for more information about SSC and SSY
316 equipments and methods. Discharge, SSC and SSY have also been measured at three other
317 stations within the catchment (i.e., Duyes River at Mallemoisson, Galabre River at Robine,
318 Bléone River at Prads) since October 2007 (see Fig. 1; Table 1). Discharge and sediment have
319 also been monitored since 1985 in the Draix Observatory managed by Irstea in Grenoble. We
320 took into consideration the data from the monitoring station of the Laval torrent (0.86 km²)
321 available since 1985 and still ongoing (Mathys et al. 2003; see Fig. 1; Table 1).

322 We also used a database of field observations made available by the office in charge of
323 mountain area restoration in France (i.e., *Restauration des Terrains en Montagne* service
324 (RTM) of the French National Forest Office; RTM, 2010). Important historical information
325 has been compiled since 1351 in the Bléone River basin (i.e., the oldest information of
326 torrential flood available): the occurrence of avalanches, rock falls, debris flows, torrential
327 floods and landslides. In this study, we extracted from this database the annual frequency of
328 debris flows/flash floods and landslides observed in the Bléone catchment since 1960 to
329 document erosion intensity within the Bléone catchment throughout time.

330

331 **4 Results and discussion**

332 **4.1 ²¹⁰Pb_{xs} and ¹³⁷Cs dating**

333 Gamma spectrometry countings conducted at Gif-sur-Yvette and Modane laboratories
334 provided very complementary results. We observed a decay of ²¹⁰Pb_{xs} with depth in the
335 sediment core when taking all 92 analysed samples into account (Fig. 4) even though
336 precision obtained on activities was larger on the 45 samples analysed in Modane, because of
337 the very low level of background at this underground laboratory (see Fig. 4). Sedimentation
338 rate could be calculated based on ²¹⁰Pb_{xs} decay of activities and was estimated at 5.4 cm yr⁻¹
339 along the first 150 cm, and at 4 cm yr⁻¹ if we take the entire depth of the core into account.

340 Activities in ^{137}Cs provided additional information to date the core. Peak activities were
341 measured between 278 and 288 cm depths (32–44 Bq kg⁻¹). Peak associated with the bomb
342 fallout (maximum activity in 1963) usually reaches values $\geq 30\text{--}35$ Bq kg⁻¹ (e.g., Le Cloarec
343 et al., 2011; Perga et al., 2010), which remains consistent with our findings. Furthermore,
344 presence of ^{241}Am (ca. 1 – 1.5 Bq kg⁻¹) could be detected at this depth (265–290 cm),
345 confirming the bomb origin of ^{137}Cs fallout. In contrast, ^{137}Cs activity peak associated with
346 Chernobyl fallout in 1986 could not be detected. This peak absence can be justified by the
347 very low cumulative rainfall amount (i.e., 9 mm) observed in the Bléone catchment when the
348 radioactive cloud flew over the area (i.e., between 30 April – 4 May according to the cloud
349 dispersion model developed by French Radioprotection and Nuclear Safety Institute (IRSN
350 2011).

351 Overall datation of the core was therefore obtained by combining the sedimentation rate
352 derived from $^{210}\text{Pb}_{\text{xs}}$ decay and the location of the bomb ^{137}Cs activity peak in depth (see Fig.
353 4c). We can note that the date of the bottom of the core corresponds to the Malijai dam
354 building (i.e., 1962). These results only provide an indicative dating of the core, as we
355 hypothesised a constant rate of sedimentation since 1962. Erosion rate varies between seasons
356 and years depending on flood magnitude. This point will be explored in detail with the hydro-
357 sedimentary interpretations.

358

359 **4.2 Stratigraphic structure of the sediment core**

360 In total, 114 varves corresponding to variations of grey shades on the X-ray images
361 were detected (Fig. 5a, b). These layers were confirmed by visual description of the core after
362 opening. Mean varve thickness reaches 2 cm, but it fluctuates between 0.2 and 13 cm. The
363 sediment core is characterised by about 7 cycles having similar stratigraphic structures, i.e. a
364 succession of several small varves (< 2 cm) followed by one to three larger varves (ranging
365 from 2–13 cm). The layer located between 91–102 cm could not be analysed because of
366 technical problems during field sampling. Oblique varves observed between 162–198 cm
367 depth cannot be attributed to a disturbance of the core during sampling or transport. We will
368 discuss its possible origin in section 5.

369

370 **4.3 Hydro-sedimentary interpretations**

371 The 1962-2009 discharge time-series available for the Bès River at Pérouré station
372 (165 km²; Fig. 6c) provide information on flood occurrence within the catchment. However,
373 because of the spatial heterogeneity of rainfall across the catchment, these data do not

374 systematically reflect the flood magnitude at the Bléone River outlet (905 km²). At the scale
375 of the entire catchment, only qualitative information about flood occurrence is available
376 (Sogreah 2005; RTM 2010; Fig. 7a). Nine major floods that led to infrastructure damages
377 have been reported by mountainous area restoration office (RTM) at the outlet of the Bléone
378 River catchment since 1970s (i.e., in July 1973, March 1974, January 1978, October 1979,
379 1992, 1993, January, September and November 1994). In January 1994, a 10-years return
380 period flood was observed (Sogreah 2004; $\sim 400 \text{ m}^3 \text{ s}^{-1}$). The peak discharge observed on the
381 Bès River at Pérouré was about $41 \text{ m}^3 \text{ s}^{-1}$ (i.e., a two-year return period flood) but the Bès
382 River subcatchment was not included in the area of maximum rainfall intensity. Two
383 additional 10-years return period floods were observed in November 1994 and 2000 at the
384 Bléone River outlet. The corresponding peak discharges observed on the Bès River at Pérouré
385 indicate that they were associated with a two-year return period at this station.
386 Furthermore, to obtain additional data at the river basin scale, we analysed the inter-annual
387 variation of rainfall based on information provided by the different rain-gauges available
388 within the catchment (see Table 1). A moving average (window size of one year; lag time of 6
389 months) was applied to monthly rainfall data (see Fig. 6a) and to the maximum daily intensity
390 of each month (see Fig. 6b). No significant pluri-annual trend could be retrieved for the 1960-
391 2009 period. We therefore defined “wet” years (i.e., with mean rainfall $> 900 \text{ mm yr}^{-1}$ and
392 mean interannual rainfall intensity $> 25 \text{ mm day}^{-1}$; see Fig. 7b) and “dry” years (i.e., with
393 mean rainfall $< 900 \text{ mm yr}^{-1}$ and mean interannual rainfall intensity $< 25 \text{ mm day}^{-1}$; see Fig.
394 7c). A pluri-annual cycle (mean period of ca. 3-5 years) with alternance/succession of “wet”
395 and “dry” years can thereby be outlined (see Fig. 7 b, c). These periods were found consistent
396 with the occurrence of large floods (Sogreah 2005; RTM 2010; see Fig. 7a), the hydrometric
397 stations records (see Table 1) and the database of the hydro-sedimentary activity (RTM 2010;
398 see Fig. 7a).

399 We can now attempt to correlate the flood deposits with inter-annual hydro-meteorological
400 patterns by a two-step count-from-the-top method (Hobo et al. 2010). In the first step, the
401 largest flood deposits were correlated with the occurrence of “wet” years and the largest
402 floods. In the second step, the smallest intermediate varves were correlated with the “wet” and
403 “dry” years that occurred between the major events. This correlation method is based on
404 several assumptions: (1) the largest floods would be responsible for the deposition of the
405 thickest varves (Hobo et al. 2010); (2) the “wet” years are the most likely periods for the
406 occurrence of large floods at the Bléone River basin scale (905 km²); (3) other small and
407 large-scale floods can also occur during the same period, but deposits from two or more

408 floods in the same hydrological season may sometimes not be identified separately. Sediment
409 deposits are indeed likely to be remobilised during the next flood, unless they are fixed by
410 vegetation during the growing season (Hobo et al. 2010); (4) ‘dry’ years can be associated
411 with small/moderate overbank floods at the core location and may result in thinner varves.

412 Varve thickness distribution matches well with the variability of the hydro-sedimentary time-
413 series (see Fig. 7d). The largest varves, i.e., between the horizons 230-260 cm, 150-220 cm,
414 80-110 cm and 30-50 cm, clearly correspond to the largest floods that occurred during the
415 “wet” periods, respectively during the periods 1968-1973, 1977-1981, 1992-1994, 1999-2002.
416 In contrast, the thinnest varves correspond to low magnitude floods that occurred during
417 “wet” and “dry” periods: 1960-1967, 1974-1976, 1982-1991, 1995-1998, 2003-2009. The
418 oblique varves observed between 160-200 cm are likely to correspond to the collapse of the
419 river bank at that location and can be associated with the widespread flood that occurred in
420 1979 (RTM 2010).

421 The grain-size fraction (<2 mm) is variable (Fig. 8a), with a dominance of silt-clay sized
422 fraction throughout the core (ca. 80%). The mean D50 is 18.5 μm (range from 0.7 - 84 μm);
423 the mean D10 is 2.3 μm (range from 0.16-22.7 μm) and the mean D90 is 160 μm (<1000
424 μm). Sand fraction is higher between 120-250 cm (ca. 30%). This core section could
425 correspond to the large floods documented during the 1970s (1973, 1978, 1979 floods; see
426 Fig. 3c) thereby confirming our previous interpretation.

427

428 **4.4 Sediment core fingerprinting**

429 Results of the mixing model showed that sediment sources varied during the last 50 years
430 for the selected core sections (see Fig. 8b). Globally, black marls and (marly) limestones
431 provided the bulk of sediment throughout the sequence: on mean 40% for black marls (min. =
432 19% and max = 71%) and on mean 22% for limestones (min = 14%; max = 34%). Major
433 floods can also generate huge quantities of sediment originating from Quaternary deposits and
434 conglomerates (respectively, 25% (min = 3%, max = 54%) and 16% (min = 6%, max =
435 28%)).

436 According to this model, black marls and limestones provided the bulk of sediment during the
437 1960s (51–88%). Then, during the 1970s, sediment origin was much more equilibrate
438 between material supplied by a mix of black marls, limestones, Quaternary deposits and
439 conglomerates. In 1972–1973, a flood was characterized by sediment originating mainly from
440 Quaternary deposits (84% of sediment), indicating the likely occurrence of mass movements
441 in the catchment. After this event (between 1974–1978), we calculated again a mixed

442 contribution of four substrate types to the Bléone River sediment with a clear dominance of
443 Quaternary deposit contribution in 1974. In 1979, a major flood occurred. At this horizon, we
444 observed a series of vertical varves, indicating the collapse of the river bank at that location.
445 Major mass movements are likely to have occurred during this period, as indicated by the
446 dominant contribution of Quaternary deposits and conglomerates to sediment deposited in
447 between 1970-1981. As reported from the hydrological time-series, rainfall data and past
448 observations (RTM 2010), this period was very active in terms of sediment transport. Several
449 other subsequent floods supplied sediment originating from Quaternary deposits and
450 conglomerates up to 1985. During the other floods that were analysed in detail, black marls
451 and (marly) limestones provided the bulk of sediment (36–85%), together with a mix of
452 conglomerates and Quaternary deposits. Deposits corresponding to 1991, 1993 and 2006 were
453 almost exclusively provided by black marls and marly limestones (74–89%). These variations
454 of sediment origin can be mainly attributed to the spatial variability of rainfall in the
455 catchment that triggered torrential floods, but also to the magnitude of the flood and its
456 capacity to remobilise the fine sediment temporarily stored in the river channel and
457 floodplain. Furthermore, the relative homogeneity of sediment composition within the core
458 (coefficient of variation of 31, 22, 61, 30% respectively for black marls, limestones,
459 Quaternary deposits, conglomerates) confirm that the core-derived information rather reflect
460 the occurrence of widespread and large-scale floods, with a contribution of all sediment
461 sources available in the catchment rather than the sediment export triggered by local storm
462 events.

463 These results are in agreement with the sediment flux time-series recorded at the Laval
464 Torrent at Draix (drainage area of 0.86 km²; Fig. 9). This site was indeed characterised by
465 massive exports of black marl material (Mathys et al. 2003) in 1992, 1994, 1996 and 2004
466 and 2006. These floods probably provided the flood deposits observed between 85-105 cm
467 depth and 28-35 cm depth in the core. For the other sites, only very limited data were
468 available and they only covered the end of the study period (i.e., 2007-2009) characterised
469 globally by a low sediment export at the Bléone outlet.

470

471 **4.5 Comparison with flood scale analyses conducted during the 2007-2009 period**

472 These results can be compared to previous findings obtained by sediment
473 fingerprinting on both riverbed and suspended material collected in the Bléone River
474 catchment during a more recent period (2007-2009; Fig. 10; Evrard et al. 2011; Navratil et al.
475 2012).

476 Analysis of the core deposits and the suspended sediment outlined very similar trends at the
477 catchment outlet (see Fig. 10). Black marl contribution clearly dominates, providing a mean
478 of 40% for the core deposits and 34% for the suspended sediment. Given this substrate only
479 occupies 10% of the total catchment area, it underlines the high erodibility of black marls
480 (e.g., Mathys et al. 2005; Poulenard et al. 2012). Limestones/marly limestones contributions
481 are also significant (mean of 22% for core deposits and 30% for suspended sediment), but
482 they remain in the same order of magnitude as the % of catchment surface that they occupy
483 (ca. 37 %). It confirms the lower erodibility of those substrates compared to black marls.
484 Analysis of core deposits and suspended sediment also remain consistent regarding
485 Quaternary deposits (21 % vs. 23%, respectively). This contribution corresponds once again
486 to the % of occurrence of those substrates within the catchment (ca. 27%). The lowest
487 contribution corresponds to conglomerate sources (mean of 13% vs. 16%), whereas it
488 occupies about 25% of the catchment. In contrast, black marls and limestones are under-
489 represented in riverbed sediment compared to their occurrence within the catchment, whereas
490 Conglomerates and Quaternary deposits are over-represented in this material.
491 The grain size of these different sources may explain this variability, even though we could
492 take those differences into account in our fingerprinting study by conducting appropriate
493 sieving. Further studies should focus on the variation of grain size of sediments during their
494 transfer across catchments in order to outline the different erosion/transfer processes that are
495 involved at different spatial and temporal scales.

496

497 **5 Conclusions**

498 We can demonstrate from our core dating study that we could reconstruct the history
499 of sedimentation since Malijai dam building by analyzing and dating a sediment core
500 collected at this location, draining a 905-km² highly erosive Alpine catchment. Determination
501 of 1963 bomb fallout peak is confirmed by the detection of ²⁴¹Am (emitted by the bombs but
502 not by Chernobyl accident). We could not detect any peak corresponding to Chernobyl fallout
503 in 1986 (which is confirmed by the very low rainfall amount observed in this catchment in
504 April – May 1986), but we could derive a mean sedimentation rate during this period,
505 providing a way to date the entire sediment core. The hydro-sedimentary interpretation
506 corroborates this analysis, and we could associate each major varve with very active erosive
507 periods that produced significant sediment exports since 1962 until 2009 at the Bléone River
508 outlet.

509 Black marls and (marly) limestones provided the bulk of sediment throughout the sequence
510 (on mean 40% and 22%, respectively) but we could outline the occurrence of major floods
511 generating huge quantities of sediment originating from Quaternary deposits and
512 conglomerates (on mean 25% and 16%, respectively). These results are consistent with the
513 ones obtained in previous studies where a similar sediment composition was found in
514 suspended sediment collected during (or after) large and widespread floods that occurred
515 between 2007 – 2009 in the Bléone River catchment. In contrast, those results slightly
516 differed with the ones derived from riverbed sediment analysis, outlining the need to take
517 account of the entire grain size range of sediment material within catchments to provide an
518 overall picture of sediment sources and transfers within highly erosive catchments.
519 Overall, this study also underlines the relevance of using archive data – i.e., hydrological
520 time-series and sediment core – to validate sediment fingerprinting analyses conducted
521 generally during short monitoring time-period (i.e., several years).

522

523 **Acknowledgements** This work was part of the STREAMS (Sediment TRansport and Erosion
524 Across Mountains) project, funded by the French National Research Agency (ANR-Blanc
525 program, BLAN06-1 139157). The authors would like to thank Grégory Bièvre and Thierry
526 Winiarski respectively from the *Laboratoire de Géophysique Interne et Tectonophysique*
527 (LGIT; UJF) and the *Laboratoire des Sciences de l'Environnement* (LSE; ENTPE); the *Eaux*
528 *Claires* Hospital of Grenoble, Frédéric Malinur, Lucas Muller, Sébastien Klotz, Manu Olivier
529 for their help during the installation of the monitoring stations, the field survey and analysis;
530 the DREAL for the data on the Bès River at Pérouré; Dominique Cordeuil and Ainhoa Mate-
531 Marin for their help during the data analysis. Louise Bordier and Juliette Montaigu are
532 gratefully acknowledged for their help for sample preparation and geochemical analyses.
533 LSCE contribution No. X.

534

535

536 **References**

537 Accornero A, Gnerre R, Manfra L (2008) Sediment concentrations of trace metals in the
538 Berre lagoon (France): an assessment of contamination. *Arch Environ Con Tox* 54:372–385
539 Antonelli C, Eyrolle F, Rolland B, Provansal M, Sabatier F (2008) Suspended sediment and
540 ¹³⁷Cs fluxes during the exceptional December 2003 flood in the Rhone River, southeast
541 France. *Geomorphology* 95(3–4):350-360

542 Appleby PG (2000) Radiometric dating of sediment records in European mountain lakes.
543 *Limnologia* 59:1–14

544 Appleby PG, Oldfield L (1983) The assessment of ^{210}Pb data from sites with varying
545 sediment accumulation rates. *Hydrobiologia* 103:29-35

546 Ayrault S, Priadi CP, Evrard O, Lefèvre I, Bonté P (2010) Silver and thallium historical
547 trends in the Seine River basin. *J Environ Monitor* 12:2177-2185

548 Blott S and Pye K (2001) Gradistat: a grain size distribution and statistics package for the
549 analysis of unconsolidated sediments. *Earth Surf Process Landforms* 26:1237–1248

550 Collins A, Walling D (2002) Selecting fingerprint properties for discriminating potential
551 suspended sediment sources in river basins. *J Hydrol* 261:218-244

552 Collins AL, Walling DE, Leeks GJL (2005) Storage of fine-grained sediment and associated
553 contaminants within the channels of lowland permeable catchments in the UK. In: Walling
554 DE, Horowitz A (eds) *Sediment Budgets*. IAHS Publication No. 291. IAHS Press,
555 Wallingford, pp 259–268

556 de Montety L, Long B, Desrosiers G, Crémer JF, Locat J, Stora G (2003) Utilisation de la
557 scanographie pour l'étude des sédiments : influence des paramètres physiques, chimiques et
558 biologiques sur la mesure des intensités tomographiques. *Can J Earth Sci* 40:937–948

559 Di Giovanni C, Disnar JR, Macaire JJ (2002) Estimation of the annual yield of organic carbon
560 released from carbonates and shales by chemical weathering. *Global Planet Change* 32:195-
561 210

562 Duvert C, Gratiot N, Evrard O, Navratil O, Prat C, Esteves M (2010) Drivers of erosion and
563 suspended sediment transport in three headwater catchments of the Mexican Central
564 Highlands. *Geomorphology* 123:243-256

565 Duvert C, Gratiot N, Nemery J, Burgos A, Navratil O (2011) Sub-daily variability of
566 suspended sediment fluxes in small mountainous catchments – Implications for community
567 based river monitoring. *Hydrol Earth Syst Sc* 15(3)703–713

568 Esteves M, Descroix L, Mathys N, Lapetite J (2005) Field measurement of soil hydraulic
569 properties in a marly gully catchment (Draix, France). *Catena* 63(2-3):282-298

570 Evrard O, Némery J, Gratiot N, Duvert C, Ayrault S, Lefèvre I, Poulenard J, Prat C, Bonté P,
571 Esteves M (2010) Sediment dynamics during the rainy season in tropical highland
572 catchments of central Mexico using fallout radionuclides. *Geomorphology* 124:42-54

573 Evrard O, Navratil O, Ayrault S, Ahmadi M, Némery J, Legout C, Lefèvre I, Poirel A, Bonté
574 P, Esteves M (2011) Combining suspended sediment monitoring, elemental geochemistry

575 and radionuclides to trace the spatial origin of fine sediment in a mountainous river
576 catchment, *Earth Surf Process Landforms* 36:1072-1089

577 Evrard O, Van Beek P, Gateuille D, Pont V, Lefèvre I, Lansard B, Bonté P (in press)
578 Evidence of the radioactive fallout in France due to the Fukushima nuclear accident. *Journal*
579 *of Environmental Radioactivity* (in press)

580 Gottardi F (2009) Estimation statistique et réanalyse des précipitations en montagne.
581 Utilisation d'ébauches par types de temps et assimilation de données d'enneigement.
582 Application aux grands massifs montagneux français. unpublished PhD thesis ; INP
583 Grenoble. 284 p

584 Hobo N, Makaske B, Middelkoop H, Wallinga J (2010) Reconstruction of floodplain
585 sedimentation rates: a combination of methods to optimize estimates. *Earth Surf. Process.*
586 *Landforms* 35:1499–1515

587 IRSN (2011) http://www.irsn.fr/FR/popup/Pages/tchernobyl_video_nuage.aspx

588 Le Cloarec MF, Bonté PH, Lestel L, Lefèvre I, Ayrault S (2011) Sedimentary record of metal
589 contamination in the Seine River during the last century. *Phys Chem Earth, Parts A/B/C*
590 36(12):515-529

591 Lenzi M.A, Mao L, Comiti F (2003) Interannual variation of suspended sediment load and
592 sediment yield in an Alpine catchment. *Hydrolog Sci J* 48:899-915

593 Lofi J and Weber O (2001) SCOPIX - digital processing of X-ray images for the enhancement
594 of sedimentary structures in undisturbed core slabs. *Geo-Mar Lett* 20:182-186

595 Mano V, Nemery J, Belleudy P, Poirel A (2009) Assessment of suspended sediment transport
596 in four Alpine watersheds (France): influence of the climatic regime. *Hydrol Process*
597 23:777-792

598 Mathys N, Brochot S, Meunier M, Richard D (2003) Erosion quantification in the small marly
599 experimental catchments of Draix (Alpes de Haute Provence, France). Calibration of the
600 ETC rainfall–runoff–erosion model. *Catena* 50:527-548

601 Mathys N, Klotz S, Esteves M, Descroix L, Lapetite J (2005) Runoff and erosion in the Black
602 Marls of the French Alps: Observations and measurements at the plot scale. *Catena* 63(2-
603 3):261-281

604 Navratil O, Legout C, Gateuille D, Esteves M, Liebault F (2010) Assessment of intermediate
605 fine sediment storage in a braided river reach (Southern French Prealps), *Hydrol Process*
606 24:1318–1332

607 Navratil O, Esteves M, Legout C, Gratiot N, Némery J, Willmore S, Grangeon T (2011)
608 Global uncertainty analysis of suspended sediment monitoring using turbidimeter in a small
609 mountainous river catchment. *J Hydrol* 398:246–259

610 Navratil O, Evrard O, Esteves M, Legout C, Ayrault S, Némery J, Mate Marin A, Ahmadi M,
611 Lefèvre I, Poirel A, Bonté P (2012) Temporal variability of suspended sediment sources in
612 an alpine catchment combining river/rainfall monitoring and sediment fingerprinting. *Earth*
613 *Surf Process Landforms*. doi: 10.1002/esp.3201

614 Owens PN, Walling DE, Leeks GJL (1999) Use of floodplain sediment cores to investigate
615 recent historical changes in overbank sedimentation rates and sediment sources in the
616 catchment of the River Ouse, Yorkshire, UK. *Catena* 36:21-47

617 Owens PN, Walling DE (2003) Temporal changes in the metal and phosphorus content of
618 suspended sediment transported by Yorkshire rivers, UK over the last 100 years, as
619 recorded by overbank floodplain deposits. *Hydrobiologia* 494:185–191

620 Owens PN, Batalla RJ, Collins AJ, Gomez B, Hicks DM, Horowitz AJ, Kondolf GM, Marden
621 M, Page MJ, Peacock DH, Petticrew EL, Salomons W, Trustrum NA (2005) Fine-grained
622 sediment in river systems: Environmental significance and management issues. *River Res*
623 *Appl* 21:693-717

624 Perga M-E, Desmet M, Enters D, Reyss J-L (2010) A century of bottom-up and top-down
625 driven changes on a lake planktonic food web: A paleo-ecological and paleo-isotopic study
626 of Lake Annecy, France. *Limnol Oceanogr* 55:803-816

627 Pont D, Simmonet J-P, Walter AV (2002) Medium-term changes in suspended sediment
628 delivery to the ocean: consequences of catchment heterogeneity and river management
629 (Rhône River, France). *Estuar Coast Shelf Sc* 54:1–18

630 Poulenard J, Legout C, Némery J, Bramorski J, Navratil O, Douchin A, Fanget B, Perrette Y,
631 Evrard O, Esteves M (2012) Tracing sources of sediments during flood events by diffuse
632 reflectance infrared Fourier-transform (DRIFT): a case study in highly erosive mountain
633 catchment (Southern French Alps). *J Hydrol* 414–415:452–462

634 Reyss J L, Schmidt S, Legeleux F, Bonté P (1995) Large, low background well-type detector
635 for measurements of environmental radioactivity. *Nucl Instrum Methods A* 357:391-397

636 RTM (2010) Restauration des Terrains de Montagne database, French Environmental
637 Ministry, BD-RTM Evénements (flash floods, debris flows, inundation, landslide,
638 avalanche, rock fall), <http://rtm-onf.ifn.fr>

639 Sempéré R, Charriere B, van Wambeke F, Cauwet G (2000) Carbon inputs of the Rhône
640 River to the Mediterranean Sea: biochemical implications. *Global Biochem Cycl* 14:669-
641 681

642 Sicre MA, Fernandes MB, Pont D (2008) Poly-aromatic hydrocarbon (PAH) inputs from the
643 Rhône River to the Mediterranean Sea in relation with the hydrological cycle: Impact of
644 floods. *Mar Pollut Bull* 56(11):1935-1942

645 Sogreah (2005) Schéma de restauration et de gestion de la Bléone et de ses affluents ; Etat des
646 lieux. Hydrology. Technical Report, 64 p

647 Valero-Garcés BL, Navas A, Machín J, Walling D (1999) Sediment sources and siltation in
648 mountain reservoirs: a case study from the Central Spanish Pyrenees. *Geomorphology* 28(1-
649 2):23-41

650

651

652 **Table and figure captions**

653 **Table 1** Summary of the meteorological and hydro-sedimentary data used in this study (SSC:
654 suspended sediment concentration; Q: discharge; R: rainfall). “R” and “STA” referred to as
655 the raingauges and hydrometric stations (Fig. 1)

656

657 **Fig. 1** Location of the study area in France, and location of the river monitoring stations
658 (STA1–STA7) and the raingauges (R1–R15) within the Bléone River catchment (Fig. A).
659 Location of the sediment coring site at the catchment outlet (Fig. B)

660

661 **Fig. 2** Geology of the Bléone River catchment and location of the river monitoring stations
662 (from Evrard et al. 2011)

663

664 **Fig. 3** Distribution of major floods (return period > 1 yr) recorded on the Bès River at Pérouré
665 station during the 1962-2009 period. Relation with the main hydro-meteorological events
666 (Fig. A). Seasonality of the major floods since 1962 (Fig. B). Regional variability of the
667 maximum annual specific discharge in the South-Eastern French Alps (Fig. C)

668

669 **Fig. 4** Sediment core dating derived from the distribution of ^{137}Cs (Fig. A) and $^{210}\text{Pb}_{\text{ex}}$ (Bq
670 kg^{-1} , Fig. B) activities with depth. Time-scale based on radionuclide dating (Fig. C)

671

672 **Fig. 5** Sediment core analysis and varve identification with X-ray intensity level (Fig. A, B).
673 Time-scale based on radionuclide dating (Fig. C)

674

675 **Fig. 6** Hydrometeorological data. Fig. A: monthly rainfall (in grey, the monthly data at the
676 different raingauges). Fig. B: maximum daily rainfall. Fig. C: discharge data of the Bès River
677 at Pérouré (daily and instantaneous discharge)

678

679 **Fig. 7** Core interpretation. Flash floods/debris flows and landslides frequency (RTM source;
680 Fig. A). Mean annual rainfall (moving average; Fig. B) and daily intensity rainfalls (moving
681 average; Fig. C). The “wet” years (black) and “dry” years (grey) are defined for each variable.
682 Varves’ thickness (Fig. D). Time-scale based on radionuclide dating (Fig. E)

683

684 **Fig. 8** Sediment size composition (Fig. A) and sediment composition with geochemistry (Fig.
685 B). Time-scale based on radionuclide dating (Fig. C)

686

687 **Fig. 9** Total sediment yield (suspended sediment and bedload) at the Laval catchment

688

689 **Fig. 10** Fine sediment origins at the Bléone River outlet. Proportion of draining catchment
690 surface occupied by the different lithologic sources (%; black bars), riverbed sediment
691 composition (%; white bars; Evrard et al. 2011), suspended sediment composition (grey bars;
692 mean \pm min./max. range of values obtained for the entire series of samples collected; Navratil
693 et al. 2012) and core composition (red bars; mean \pm min./max; this study)

Fig. 1 Location of the study area in France, and location of the river monitoring stations (STA1–STA7) and the raingauges (R1–R15) within the Bléone River catchment (Fig. A). Location of the sediment coring site at the catchment outlet (Fig. B)

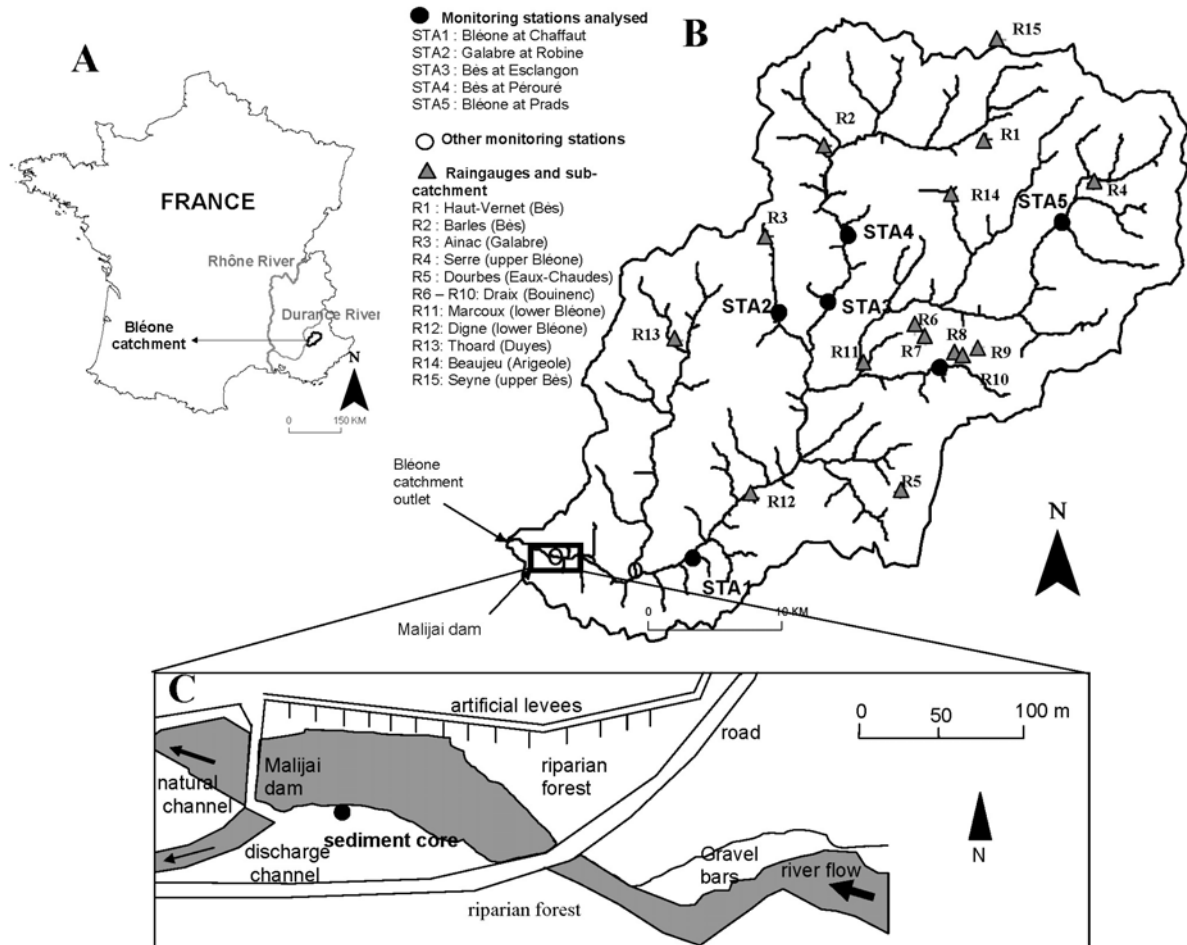


Fig. 2 Geology of the Bléone River catchment and location of the river monitoring stations (from Evrard et al. 2011)

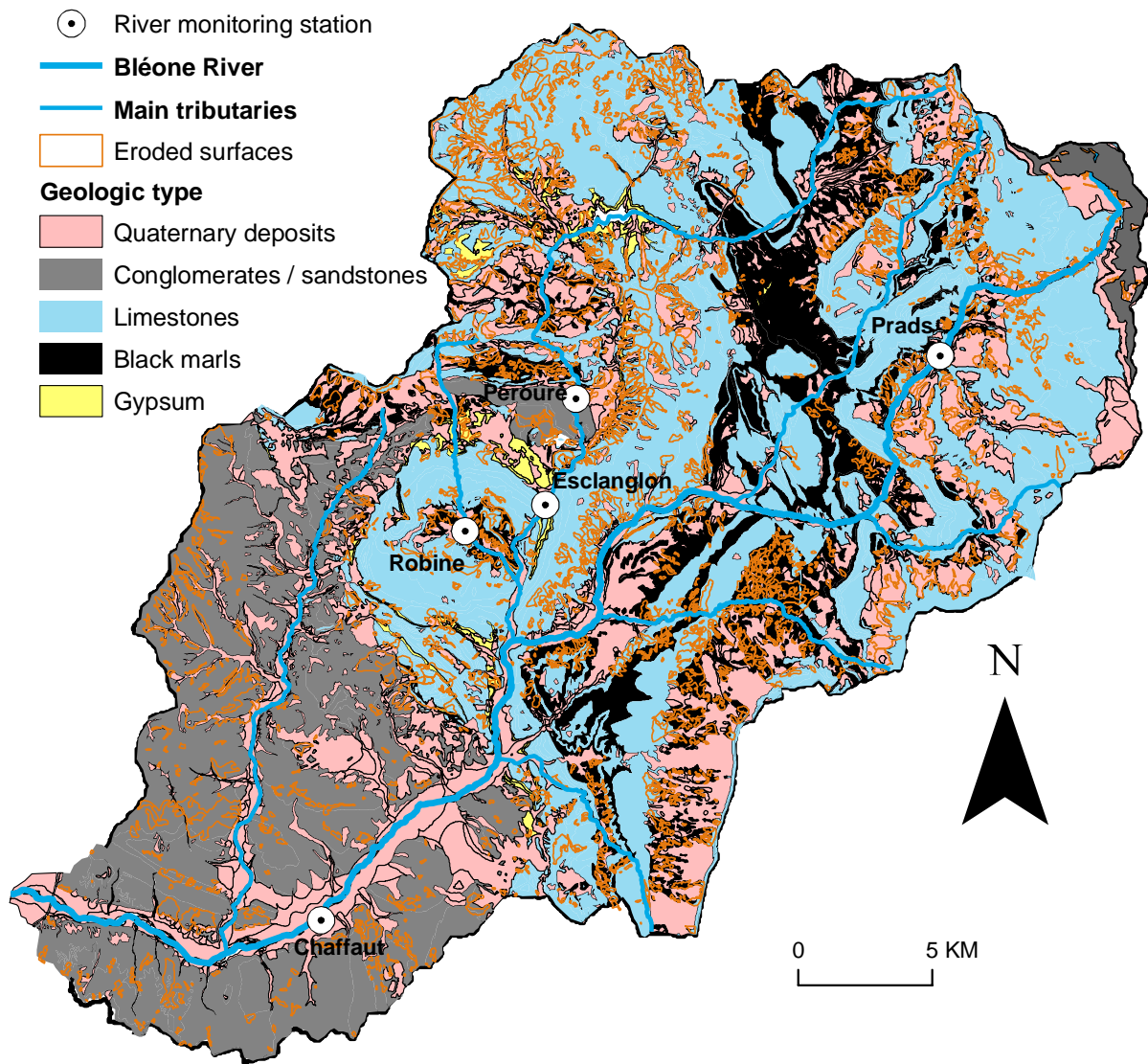


Fig. 3 Distribution of major floods (return period > 1 yr) recorded on the Bès River at Pérouré station during the 1962-2009 period. Relation with the main hydro-meteorological events (Fig. A). Seasonality of the major floods since 1962 (Fig. B). Regional variability of the maximum annual specific discharge in the South-Eastern French Alps (Fig. C)

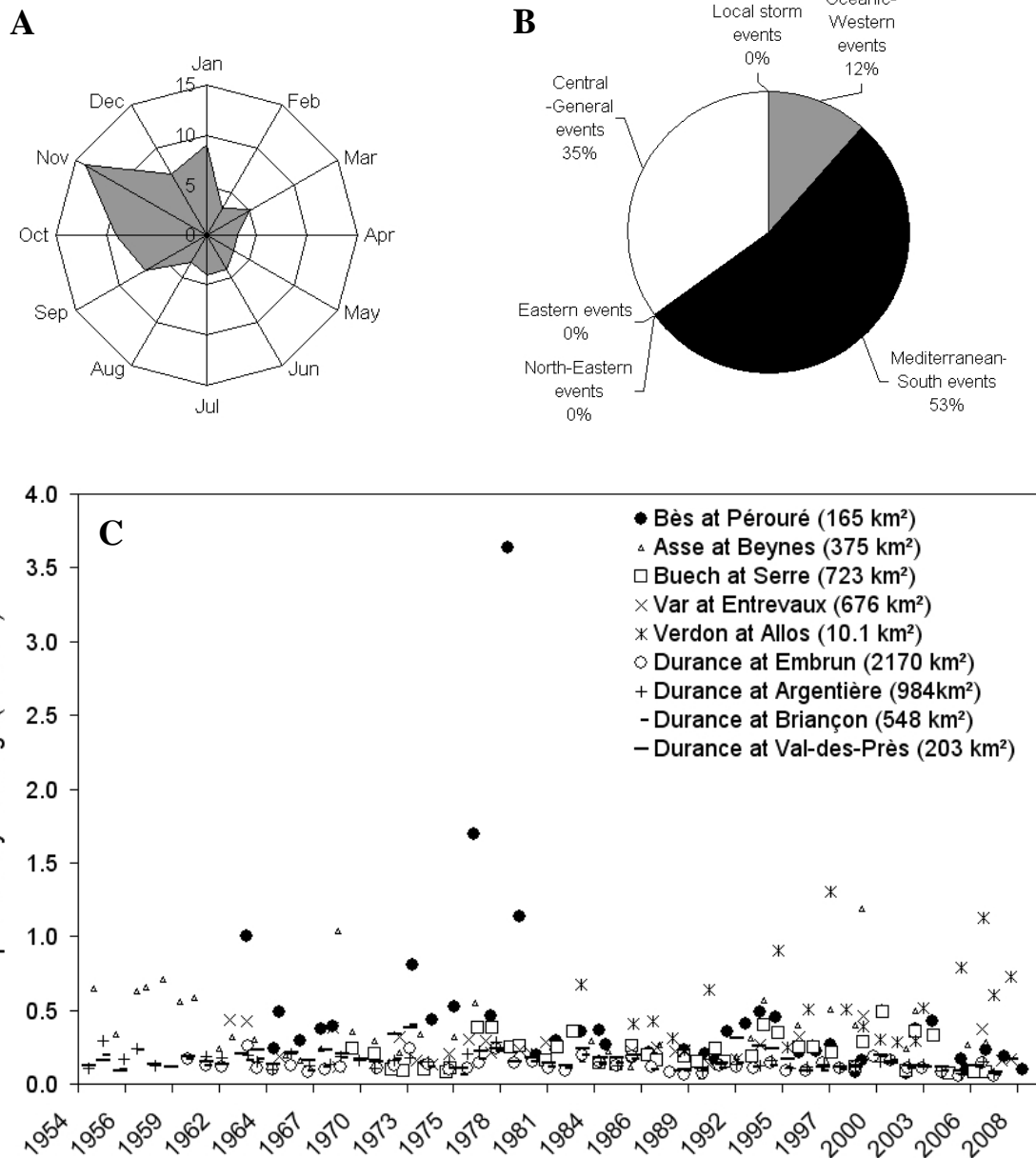


Fig. 4 Sediment core dating derived from the distribution of ^{137}Cs (Fig. A) and $^{210}\text{Pb}_{\text{xs}}$ (Bq kg^{-1} , Fig. B) activities with depth. Time-scale based on radionuclide dating (Fig. C)

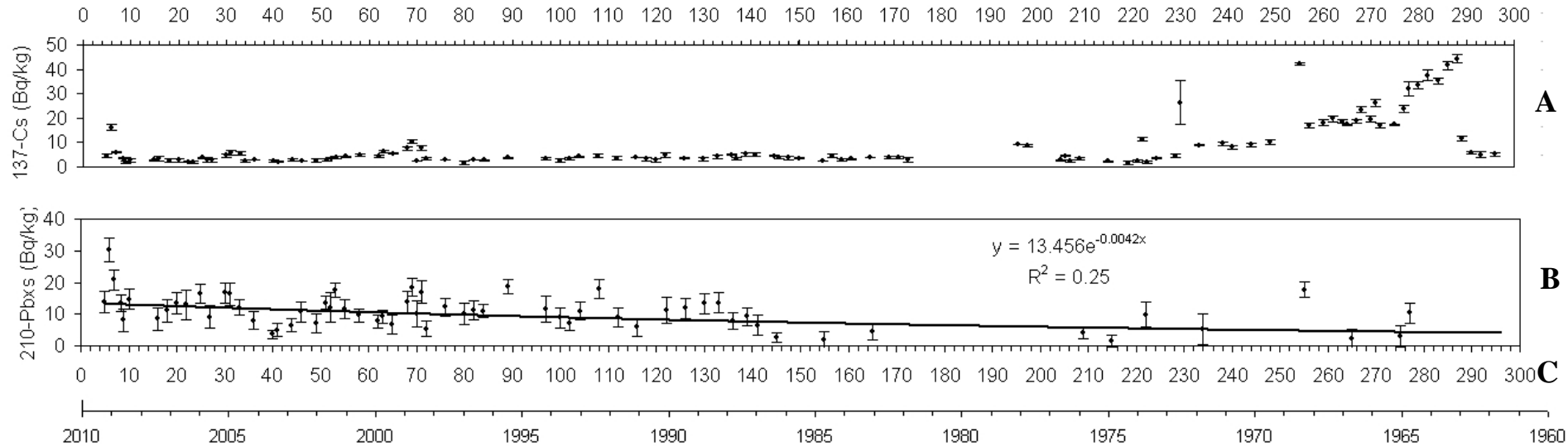


Fig. 5 Sediment core analysis and varve identification with X-ray intensity level (Fig. A, B). Time-scale based on radionuclide dating (Fig. C)

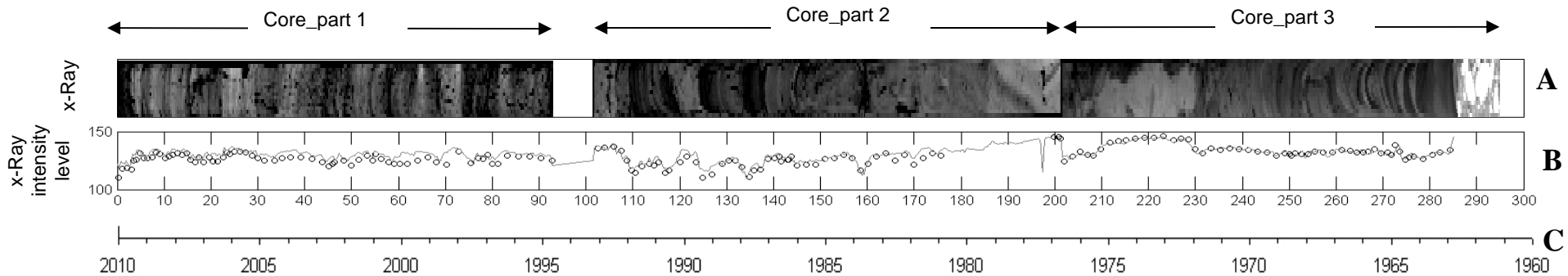


Fig. 6 Hydrometeorological data. Fig. A: monthly rainfall (in grey, the monthly data at the different raingauges). Fig. B: maximum daily rainfall. Fig. C: discharge data of the Bès River at Pérouré (daily and instantaneous discharge)

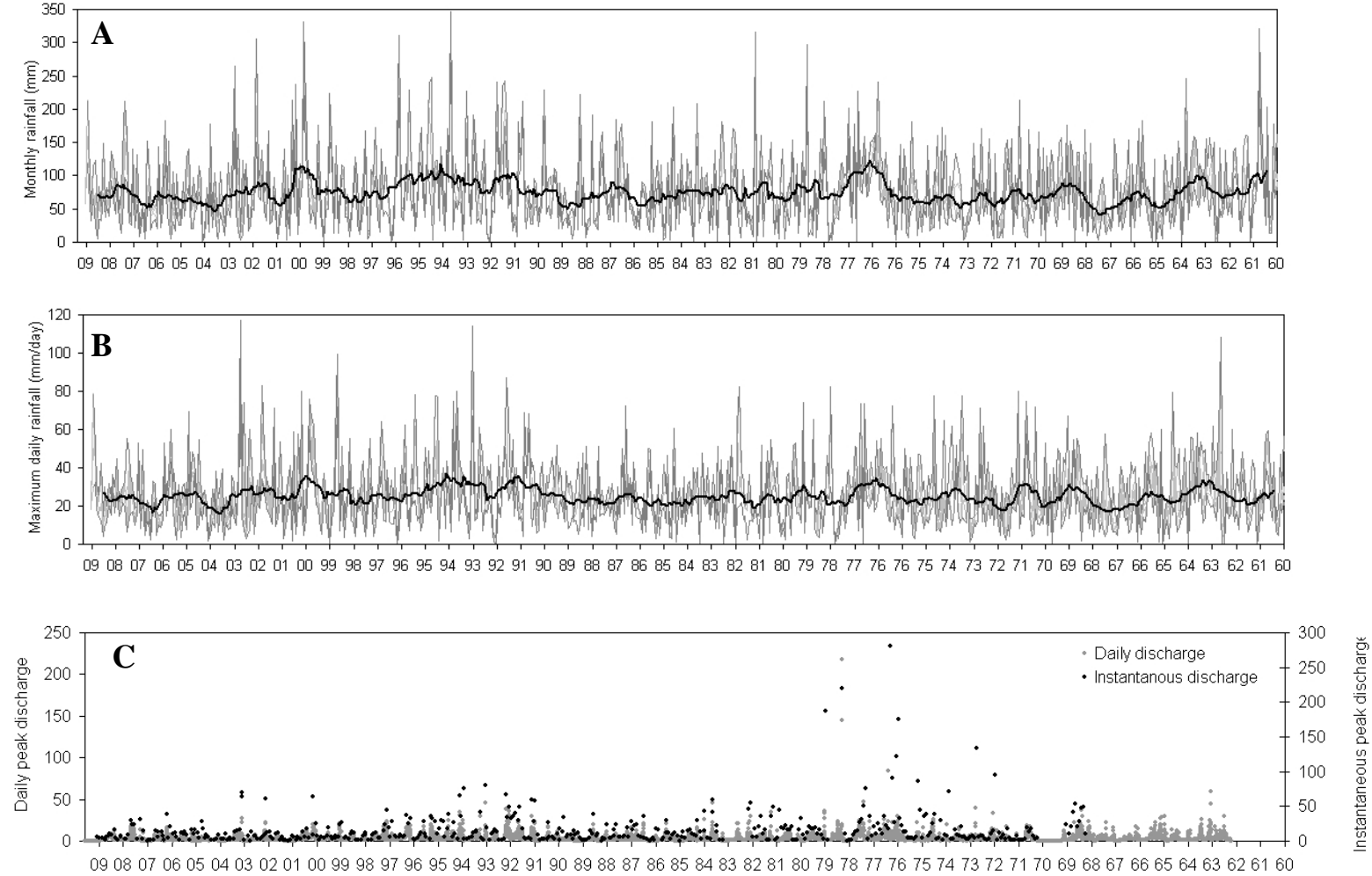


Fig. 7 Core interpretation. Flash floods/debris flows and landslides frequency (RTM source; Fig. A). Mean annual rainfall (moving average; Fig. B) and daily intensity rainfalls (moving average; Fig. C). The “wet” years (black) and “dry” years (grey) are defined for each variable. Varves’ thickness (Fig. D). Time-scale based on radionuclide dating (Fig. E)

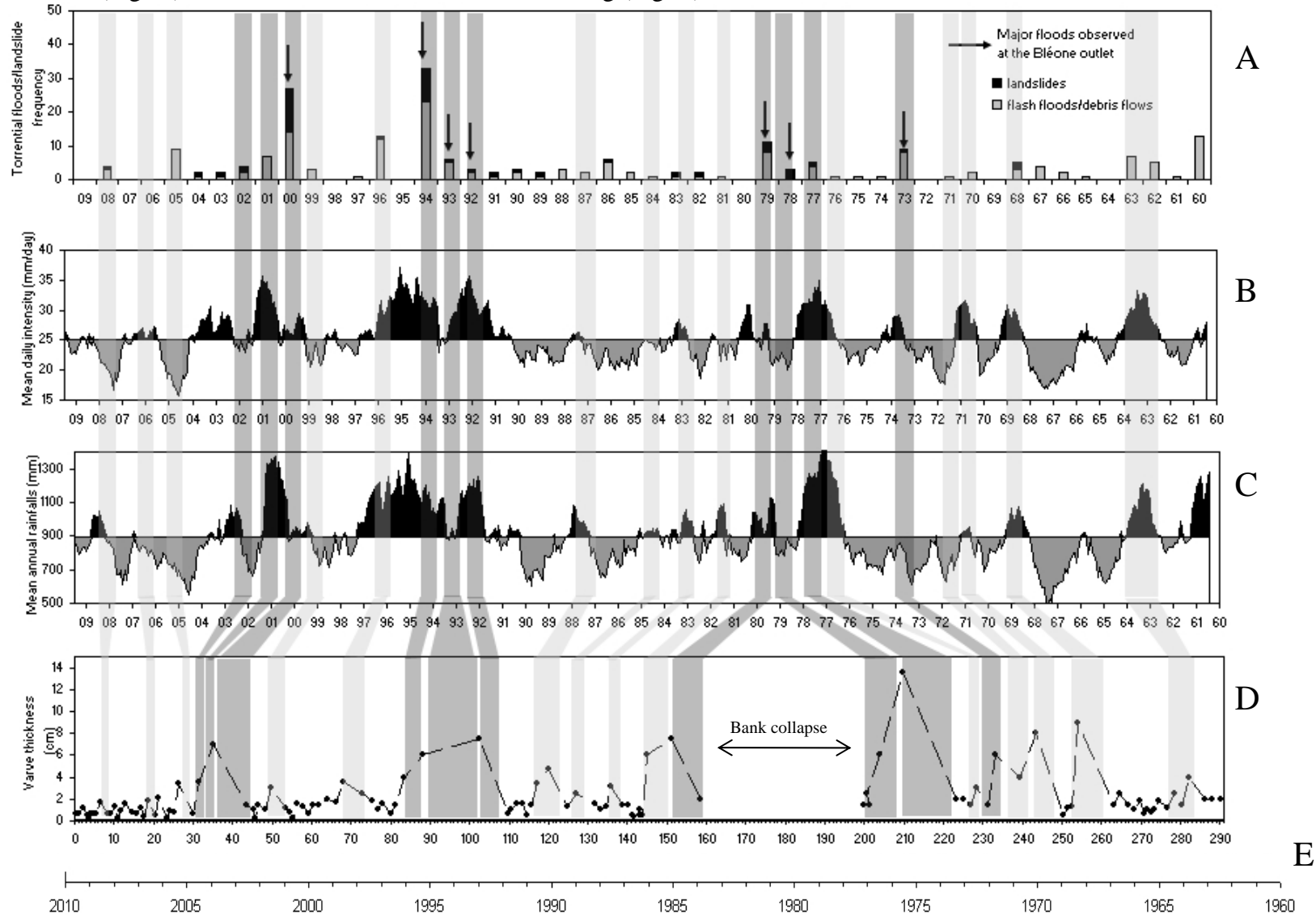


Fig. 8 Sediment size composition (Fig. A) and sediment composition with geochemistry (Fig. B). Time-scale based on radionuclide dating (Fig. C)

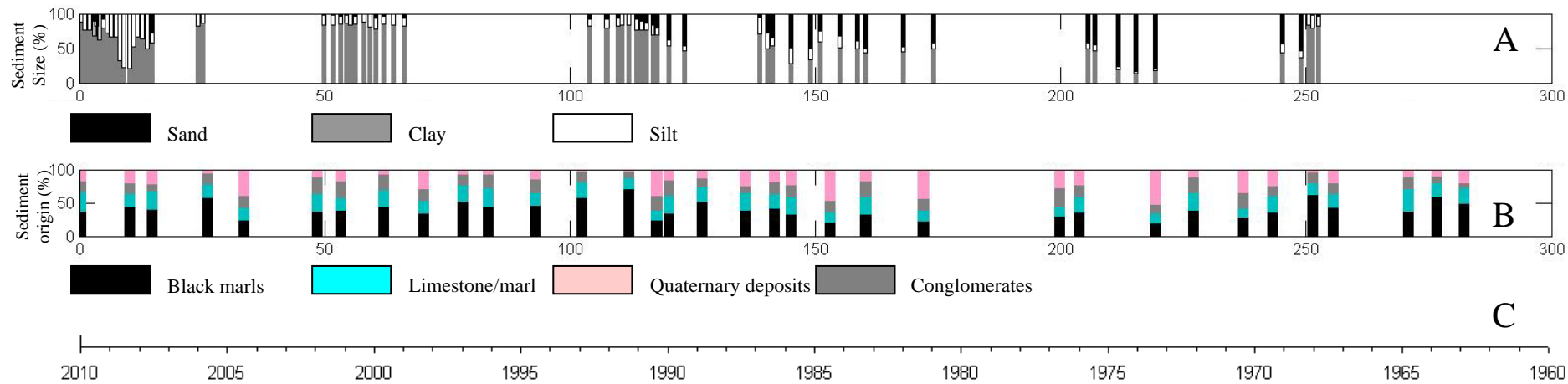


Fig. 9 Total sediment yield (suspended sediment and bedload) at the Laval catchment

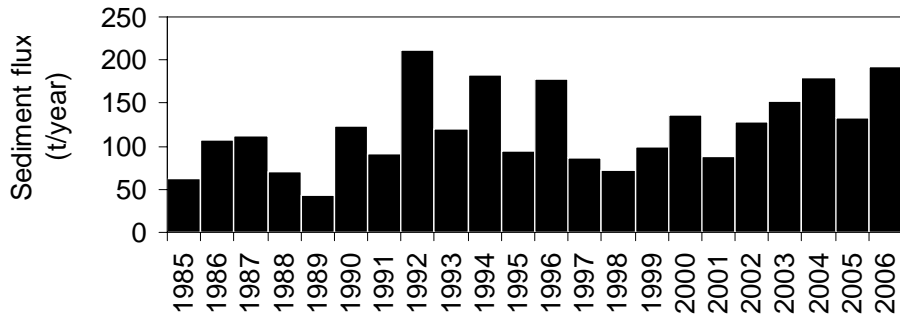
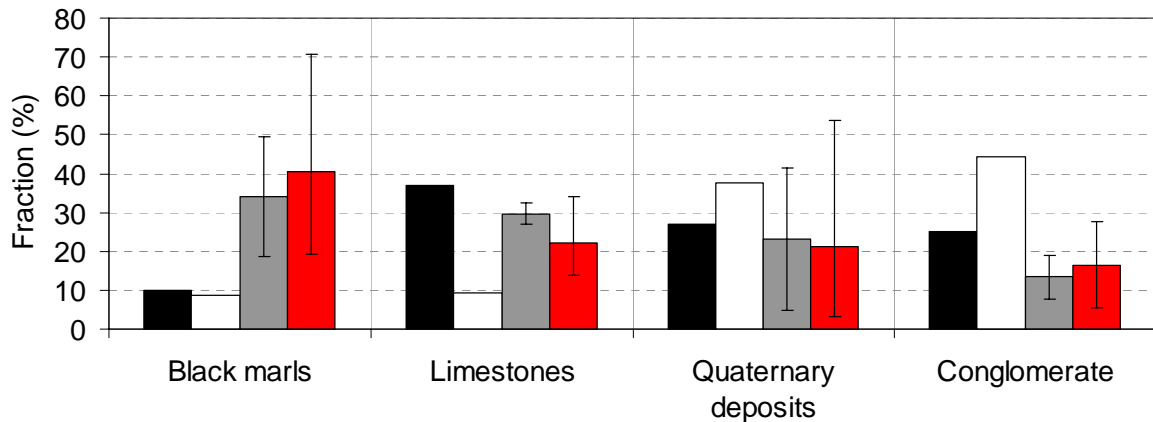


Fig. 10 Fine sediment origins at the Bléone River outlet. Proportion of draining catchment surface occupied by the different lithologic sources (%; black bars), riverbed sediment composition (%; white bars; Evrard et al. 2011), suspended sediment composition (grey bars; mean \pm min./max. range of values obtained for the entire series of samples collected; Navratil et al. 2012) and core composition (red bars; mean \pm min./max; this study)



Tab. 1 Summary of the meteorological and hydro-sedimentary data used in this study (SSC: suspended sediment concentration; Q: discharge; R: rainfall). “R” and “STA” referred to as the raingauges and hydrometric stations (Figure 1)

Basin name	Station location	Drainage area (km²)	Data type	Observation period	Station manager
Laval	Draix	0.86	Q, SSC (variable time step) STA8, R6 to R10 (5. min.)	1984-2010	Cemagref Grenoble/ETNA
Bès	Pérouré	165	Q, SSC (10. min.) ; STA3; STA4	1962- 2010 for Q 2007- 2010 for SSC	SPC Grand Delta, DIREN, EDF-DTG, LTHE
Duyes	Mallemoisson	120	Q, SSC (10. min.) STA 6	2007-2010	LTHE
Galabre	Roubine	22	Q, SSC (10. min.) STA2	2007-2010	LTHE
Bléone	Prads	65	Q, SSC (10. min.) STA5	2007-2010	LTHE
Bléone	Chaffaut	705	SSC (hourly) STA1	2001-2003 ; 2007-2010	EDF-DTG
Bléone	Malijai	870	Q (hourly) ; STA7	2007-2010	EDF-DTG
Arigéole	Beaujeu	---	R (daily); R14	1926-2010	Météo France
Bléone	Digne	---	R (daily); R12	1945-2010	Météo France
Bès	Seyne	---	R(daily); R15	1928-2010	Météo France
Duyes	Thoard	---	R(daily); R13	1999-2010	Météo France
Bléone	Marcoux	---	R(hourly); R11	1938-2010	Météo France
Bès	Haut-Vernet	---	R (5 min.) ; R1	2008-2010	LTHE
Bès	Barles	---	R (5 min.) ; R2	2008-2010	LTHE
Galabre	Ainac	---	R (5 min.) ; R3	2008-2010	LTHE
Bléone	Serre	---	R (5 min.) ; R4	2008-2010	LTHE
Bléone	Les Dourbes	---	R (5 min.); R5	2008-2010	LTHE
Bès	Barles	---	R (5 min.) ; R2	2008-2010	LTHE

Tab. 2 Concentrations in geochemical elements (mg kg⁻¹) and mean radionuclide activities (in Bq kg⁻¹, except for K – in %) analysed in the sediment core sections (n=34)

Section n°	Core depth																		
	(cm)	Mg	Al	Ti	Mn	V	Ni	Cu	Ag	Cd	Sb	Ba	TI	Pb	K (%)	Th-234	Ra-226	Ra-228	Th-228
1	5.4	9055	6.6	3647	463	103	50	24	0.16	0.16	0.39	376	0.54	13	1.70	31.1	22.0	32.8	35.0
2	13.4	8463	4.8	3550	582	88	38	20	0.21	0.18	0.36	349	0.38	12	1.59	28.8	22.5	30.6	30.9
3	18.7	10005	6.5	3422	458	102	45	19	0.15	0.14	0.29	273	0.47	13	1.79	26.4	23.0	34.3	32.2
4	27	9348	5.8	4230	680	104	44	20	0.17	0.13	0.34	305	0.43	13	1.55	30.0	23.0	31.6	32.0
5	33.2	6168	5.2	2688	393	81	40	23	0.21	0.14	0.32	446	0.38	12	1.29	24.3	22.0	29.0	27.1
6	45.7	8535	4.0	2917	705	70	39	21	0.19	0.14	0.36	266	0.29	14	1.28	23.9	20.0	28.1	25.9
7	49.7	10306	5.5	3192	568	83	45	20	0.20	3.25	0.42	244	0.37	53	1.27	23.0	20.0	28.4	26.3
8	56.9	8315	4.9	3473	689	88	42	23	0.22	0.14	0.61	359	0.38	13	1.44	30.0	24.0	28.0	30.0
9	65.5	10735	5.1	2929	455	86	43	18	0.15	0.14	0.39	232	0.38	13	1.40	23.9	22.5	28.7	28.6
10	70.8	8211	6.3	4221	580	114	46	26	0.24	0.19	0.54	446	0.53	13	1.63	25.2	26.0	32.4	31.0
11	74.5	8598	4.7	3173	739	82	41	19	0.25	0.14	0.42	259	0.36	13	1.49	19.4	22.5	29.0	28.9
12	84.0	9768	5.8	3210	579	92	44	20	0.27	0.13	0.40	267	0.40	14	1.37	21.0	20.0	28.9	27.8
13	100	9021	5.0	3925	815	94	43	19	0.23	0.14	0.37	292	0.36	13	1.37	21.9	20.0	28.2	28.3
14	109.1	10028	7.8	4842	681	135	44	18	0.45	0.14	0.79	323	0.58	13	1.62	28.5	23.0	35.0	31.1
15	116.4	7221	3.6	1868	489	59	37	18	0.16	0.13	0.39	262	0.26	14	0.88	13.1	19.0	18.6	16.9
16	117.6	7740	3.1	2553	677	59	34	19	0.22	0.15	0.44	254	0.25	12	0.88	13.1	16.0	18.6	16.9
17	123.6	8312	5.1	3795	610	98	41	19	0.29	0.17	0.41	332	0.39	12	2.02	26.3	24.0	33.0	35.7
18	133.0	9406	6.5	3366	433	101	44	19	0.26	0.13	0.36	342	0.47	13	1.63	27.3	21.0	32.4	30.4
19	139.5	8063	4.3	3183	623	80	35	19	0.16	0.17	0.35	315	0.36	12	1.14	22.3	20.0	25.7	22.6
20	142	7579	3.3	2707	628	65	31	17	0.14	0.16	0.29	301	0.28	10	1.13	18.5	18.5	21.1	21.5
21	150.0	7270	3.1	1654	457	48	32	16	0.12	0.11	0.41	256	0.23	12	0.84	16.2	17.0	17.2	17.1
22	157.5	7889	2.8	2349	666	53	34	19	0.17	0.14	0.38	268	0.23	12	0.97	16.7	17.0	21.1	19.5
23	169.5	6995	3.0	1642	471	43	34	17	0.15	0.12	0.44	258	0.22	12	0.87	11.9	17.0	18.7	18.5
24	198.0	9490	4.3	2384	509	78	40	24	0.15	0.13	0.40	268	0.31	15	1.20	21.9	21.0	25.0	24.1
25	207.5	8381	4.2	2676	615	70	33	18	0.23	0.13	0.33	289	0.33	12	1.10	18.4	17.0	18.0	19.2
26	223.0	5620	2.0	914	430	27	26	10	0.04	0.10	0.25	170	0.16	9	0.67	10.4	13.0	11.9	10.8
27	231	7831	3.1	2843	711	66	36	20	0.16	0.17	0.54	246	0.28	15	0.92	13.1	15.0	17.5	16.0
28	241.0	8335	4.1	2282	483	72	39	19	0.15	0.13	0.36	261	0.30	14	1.11	23.8	20.0	24.4	23.9
29	247	9186	4.5	2988	610	72	33	17	0.19	0.14	0.37	286	0.31	11	1.23	23.4	20.5	24.0	24.4
30	255.5	8797	6.1	4093	670	114	47	21	0.21	0.17	0.38	366	0.50	13	1.47	24.5	21.0	27.9	27.3
31	260.0	9712	5.4	2918	523	93	43	19	0.14	0.18	0.36	290	0.39	14	1.59	23.9	23.0	30.6	29.9
32	275.3	10269	6.2	3292	524	98	48	23	0.12	0.18	0.38	382	0.49	15	1.72	27.2	29.0	30.2	31.0
33	280.8	9916	6.2	3818	620	110	42	18	0.21	0.14	0.47	366	0.59	12	1.81	20.1	23.0	31.8	30.5
34	286	12017	6.1	3743	500	105	40	15	0.22	0.13	0.50	307	0.57	12	2.07	30.4	23.0	36.1	36.7